Available online at www.sciencedirect.com

ScienceDirect

Procedia Engineering 00 (2016) 000–000

Procedia Engineering

www.elsevier.com/locate/procedia

1st International Conference on the Material Point Method, MPM 2017

# Application of a second-order implicit material point method

Markus Bürg[a,*], Liang Jin Lim[a], Ronald Brinkgreve[a,b]

[a]*Plaxis bv, Delft, The Netherlands*
[b]*Delft University of Technology, Faculty of Civil Engineering and Geosciences, The Netherlands*

**Abstract**

In this work, we present the application of a newly developed implicit second-order Material Point Method (MPM) on offshore geotechnical applications. The presented second-order MPM uses a special set of piecewise quadratic shape functions to circumvent the well-known issue of producing zero nodal mass contributions. To mitigate the effect of the standard MPM to produce highly oscillating stresses across cell interfaces, we have carried over our ideas obtained from the derivation of the second-order MPM to the Dual Domain Material Point (DDMP) Method, too. The resulting second-order DDMP Method produces a smoother stress distribution across the entire computational domain while being able to profit from the improved convergence rates of second-order finite elements. In a numerical example from geotechnical engineering applications, we illustrate the practical application of our enhanced Material Point and DDMP Methods by simulating a cone penetration.

Peer-review under responsibility of the organizing committee of the 1 st International Conference on the Material Point Method.

*Keywords:* material point method; DDMP; large deformations; particle-in-cell method; offshore geotechnical engineering.

## 1. Introduction

The standard finite element method (FEM) has been used successfully for several decades to predict the deformation of soil in geotechnical engineering. However, for certain applications involving very large deformations, the use of standard FEM is rather cumbersome, because some cells exhibit a too large distortion and, thus, remeshing has to be performed. Particle-in-cell methods and, in particular the Material Point Method (MPM) have proven to be an adequate replacement of FEM in these types of applications [1-5]. MPM was first introduced

* Corresponding author.
*E-mail address:* mb@plaxis.nl


Peer-review under responsibility of the organizing committee of the 1 st International Conference on the Material Point Method.

by Sulsky et al. [6] and has been used in various geotechnical applications, such as modelling of landslides, cone penetration [7], pile penetration [8], spudcan penetration [2], and pipeline movement [9].

Unfortunately, due to locking effects, employing a first-order FEM for these types of analyses is not straightforward [10]. Since MPM uses a standard FEM calculation for obtaining the deformations in each time step, also the first-order MPM inherits these locking effects. One way to mitigate this issue in FEM is to use second-order shape functions. In particular, this approach has the additional benefit of improving the accuracy of the numerical solution without having the need for using a finer mesh. Unfortunately, for MPM, this approach cannot be taken over one-to-one, since the nodal mass contributions for the widely used Lagrangian shape functions (see, e.g., [11]) are zero in this case. Therefore, we will present a way to modify these Lagrangian shape functions such that this issue is resolved.

As it is the case for the standard first-order MPM, also the gradients the modified shape functions of the derived second-order MPM are discontinuous across cell interfaces. This leads to inaccurate stresses when a material point crosses from one cell to another [12-15]. To mitigate this effect, we enhance the DDMP method presented in [13] to employ our modified Lagrangian shape functions. This gives us a second-order DDMP method which possesses a much smoother stress distribution than the standard first-order as well as the previously developed second-order MPM.

This paper is structured as follows: In Section 2, we present our MPM formulation and discretise it by employing a second-order finite element approach. The DDMP method and its discrete formulation are discussed in Section 3. In Section 4, we present shortly the additional features of our MPM algorithm necessary for the applications provided in this paper. Finally, in Section 5, we show the applicability of our MPM and DDMP formulations by means of a detailed numerical example involving a cone penetration into cohesive soil.

## 2. 2. Material point method formulation

In this work, we use an implicit formulation of MPM as presented by Sulsky et al. in [16]. This has the advantage that the maximum time step size is not limited from above by a CFL condition. Nonetheless, all the ideas presented in this section can be carried over to the explicit formulation without any modification.

### *2.1. Governing continuum equations*

For a continuous body $\Omega \subset \mathbf{R}^{\mathbf{d}}$, $d \in \{2,3\}$, the conservation equations for mass and linear momentum for governing the continuous body can be defined as

$$\frac{d\rho}{dt} + \rho\nabla \cdot \frac{du}{dt} = 0 \tag{1}$$

$$\rho\frac{d^2u}{dt^2} = \nabla \cdot \sigma + \rho b, \tag{2}$$

where $\rho$ is the mass density, **u** the displacement, $\sigma$ the Cauchy stress tensor, and **b** the specific body force.

### *2.2. Discretisation of continuum equations*

The weak form of the second equation (2) can be in the standard way by multiplying with a test function and performing integration by parts [10]. It reads to find $\mathbf{u} \in \mathbf{V}$ such that

$$\int_\Omega \rho\phi\frac{d^2u}{dt^2} = f_{ext} - f_{int}, \tag{3}$$

where $\partial\Omega$ denotes the boundary of $\Omega$, $\phi \in \mathbf{V}$ are the finite element test functions. Further,

$$f_{int} := \int_\Omega \nabla\phi : \sigma \tag{4}$$

denotes the internal force and

$$f_{ext} := \int_\Omega \rho\, \phi \cdot b + \int_{\partial\Omega} \phi \cdot t \tag{5}$$

the external force, where **t** is the applied surface traction. Then, equation (3) provides a finite element discretisation of (2).

For deriving the MPM discretisation of equation (2), we have to go one step further. As in conventional FEM, the integrals are approximated by summing the weight contributions of each material point. For the standard first-order MPM as presented in [6], the approximation of the integral of an arbitrary function $F$ over domain $\Omega$ is given by

$$\int_\Omega F \approx \sum_{p=1}^{N_p} v_p\, F(x_p), \tag{6}$$

where $N_p$ denotes the number of material points and $v_p$ and $\mathbf{x}_p$ denote the volume and the position, respectively, of material point $p$. The internal force $\mathbf{f}_{int}$ can then be approximated by

$$f_{int} \approx \sum_{p=1}^{N_p} v_p\, \nabla\phi : \sigma(x_p) \tag{7}$$

*2.3. Implicit time integration scheme*

Solving a single step in MPM is identical to the solution procedure of the conventional FEM. We employ a Newton method for solving the nonlinear equation of motion (2). In this case, the linear system which has to be solved during a Newton iteration $n$ is given by

$$A(u_{n-1})\Delta u_n = f_{ext} - f_{int}(u_{n-1}) - M a_{n-1}, \tag{8}$$

where the tangent matrix **A** and the internal force $\mathbf{f}_{int}$ both depend on the displacement $\mathbf{u}_{n-1}$ from the previous iteration, $\Delta\mathbf{u}_n$ denotes the sought displacement increment in the current iteration, and $\mathbf{a}_{n-1}$ is the acceleration from the previous iteration. Then, the displacement of the current iteration $n$ can be calculated by

$$u_n = u_{n-1} + \Delta u_n \tag{9}$$

The acceleration can be computed by discretising the time derivative with the Newmark constant average rule. Then, the discretised acceleration $\mathbf{a}_n$ and velocity $\mathbf{v}_n$ are given by

$$a_n = \frac{4}{\Delta t^2} u_{n-1} - \frac{4}{\Delta t} v_{n-1} - a_{n-1} \quad \text{and} \quad v_n = v_{n-1} + \frac{2}{\Delta t}\Delta u_n - v_{n-1}, \tag{10}$$

where $\mathbf{a}_0$ and $\mathbf{v}_0$ are acceleration and velocity at the start of the time step, respectively.

In contrast to the conventional FEM, all the state variables are stored in the material points at the beginning of each calculation step. These state variables have to be interpolated to the computational grid. For the standard first-order MPM, usually standard shape function interpolation is used. In this case, the nodal velocity at node $i$ is given by the conservation of momentum equation

$$m_i v_i = \sum_{p=1}^{N_p} \rho\, v_p \phi_i(x_p) v_p \tag{11}$$

Unfortunately, in case of constant velocity $\mathbf{v}_p$, the nodal velocity $\mathbf{v}_i$ will be zero for all degrees of freedom being located on the cell vertices, when standard second-order Lagrangian shape functions are used. This is the case because those second-order shape functions have a positive and a negative part which cancel each other out when simply being added. In conventional FEM, this is not an issue, since the loop runs over the degrees of freedom, whereas in equation (11) it is over the material points. Therefore, we define a new set of second-order shape

functions which do not exhibit this behaviour. Let $\{\phi_i\}_{i=1,\dots,N}$ be the set of all Lagrangian shape functions. Further, the positive part of $\phi$ is denoted by $\phi+_i$ . Then, the nodal velocity can be obtained in the same way as in (11), where we just replace the standard Lagrangian shape functions by its positive part:

$$m_i v_i = \sum_{p=1}^{N_p} \rho\, v_p \phi_i^+(x_p) v_p \tag{12}$$

This way, we obtain a well-defined nodal velocity. In particular, it is worth noting that for first-order shape functions as well as all-positive second-order shape functions, we simply recover the standard definition of the nodal velocity.

After the Newton procedure has obtained a sufficiently accurate numerical solution, a convective stage is carried out in the MPM region. This stage updates the state variables from the computational grid back onto the material points. Once the convective stage is completed, the deformed computational grid can be discarded, since all the state information is now stored in the material points. As a result, excessive mesh distortion is prevented.

## 3. Dual domain material point method formulation

The dual domain material point (DDMP) method is an enhancement of the conventional MPM and has been presented in [13]. It uses a modified gradient of the shape functions to eliminate the noise and instabilities occurring when material points cross over cell interfaces.

In [13], the nodal volume $V_i$ has been defined by the formula

$$V_i := \int_\Omega \phi_i \qquad \forall i = 1,\dots,N \tag{13}$$

As, we have observed in Section 2, this nodal volume will be zero for the second-order Lagrangian shape functions $\phi_i$ located on the cell vertices of the mesh. Therefore, we modify this definition in the same way as in Section 2 and use the positive part of the shape function to obtain the modified nodal volume

$$\tilde{V}_i := \int_\Omega \phi_i^+ \qquad \forall i = 1,\dots,N \tag{14}$$

Again, for first-order shape functions and all-positive second-order shape functions, we recover the original nodal volume $V_i$. With this definition at hand, let us introduce the continuous gradient

$$\tilde{\nabla}\phi_i(x) := \sum_{j=1}^{N} \frac{\phi_j(x)}{\tilde{V}_j} \int_\Omega \phi_j \nabla \phi_i \tag{15}$$

Since neither the modified nodal volume nor the integral depend on **x**, it is easy to see that this gradient is indeed continuous. However, using this smooth gradient directly in our calculations will introduce a stability issue as has been noted in [13]. To resolve this issue, we define the modified gradient

$$\bar{\nabla}\phi_i(x) := \alpha(x)\nabla\phi_i(x) + (1-\alpha(x))\tilde{\nabla}\phi_i(x)\,, \tag{16}$$

where the weight function $\alpha$ is given by

$$\alpha(x) = \frac{1}{2}\left(\prod_{k=1}^{n_c} (2\phi_{c,k}^+(x)\right)^{\frac{3}{2d(n_c-1)}} \tag{17}$$

Here, $n_c$ denotes the number of nodes of the cell K containing **x**, $\phi_{c,k}^+$ is the positive part of the $k^{\text{th}}$ Lagrangian shape function defined on cell K, and $d$ is the dimension of the problem, i.e., 2 or 3 in our case. Now, this modified gradient is used everywhere in the MPM calculation instead of the conventional gradient of the Lagrangian shape functions. For example, the approximation of the internal force $\mathbf{f}_{\underline{int}}$ from equation (7) now reads

$$f_{int} \approx \sum_{p=1}^{N_p} v_p \, \bar{\nabla}\phi : \sigma(x_p) \tag{18}$$

## 4. Additional features of material point method implementation

In this section, we present the additional features which we have added to our implementations of the MPM and DDMP method to ensure and improve its robustness, accuracy, and usability.

### *4.1. Dealing with empty cells*

When all material points have left a cell, the cell has no stiffness or mass contributions in the global matrix. To avoid singularity of the system of equations, a small elastic stiffness is put into these empty cells. This procedure is also applied to 'buffer' cells (for example above the soil surface) that are initially empty, but are present to catch material points that are moving above the initial surface. This way, we do not have to fully eliminate the degrees of freedom belonging to these empty cells and, thus, avoid a costly resize of the sparse tangent matrix in every time step.

### *4.2. Combination of FEM and MPM regions*

Since MPM and DDMP are computationally rather expensive, it should be used only where really necessary, i.e., where large deformations occur. Parts of the domain that undergo relatively small deformations can be modelled by conventional FEM using an updated Lagrangian formulation. This means that the FEM domain as well as the MPM domain can deform. Hence, the convection Phase involves an elastic stretch of the MPM mesh (adhering to the deformations of the FEM mesh), rather than a full restoration of the original grid.

In the FEM domain, conventional quadrature points are used for computing the integrals, while the MPM domain uses material points as quadrature points. The analysis procedure remains the same, except that, at the end of each calculation step, a mesh relaxation procedure is performed in the MPM domain to restore the deformed mesh in addition to the convection step of MPM. An artificial constraint is added to the FEM domain to prevent the mesh in the FEM domain from restoring, while the mesh in the MPM domain is relaxed back to its least deformed state by removing external loads contributing to the system. In this way, the mesh distortion problem in the MPM domain can be mitigated, while maintaining the validity of the deformation state of the FEM domain.

This combination approach can lead to a significant improvement in performance given the fact that a single MPM step takes about as long as three FEM steps. Consequently, the reduction of the MPM domain by half has the potential to speed up the entire calculation by about one third.

### *4.3. Contact formulation*

Although, MPM-to-MPM contact is implicitly available in the standard MPM algorithm, we chose to implement a special MPM-to-FEM contact algorithm. The major reasons for this step are the rough nature of pure MPM-to-MPM contact as well as the computational efficiency gained by being able to model the penetrating structures as pure FEM domains. The algorithm for contact interaction between a structure, modelled with FEM, and MPM based soil was initially introduced in [17]. It is based on the minimisation of the energy functional with a Lagrange multiplier and formulated as in classical contact mechanics. However, instead of employing a distance function between two contacting bodies, we use a density-based level-set function given by which marks the boundary of the material points. This can be achieved by computing the density of material points per node and, then, subtracting a small number such that the zero isosurface coincides with the boundary of the material point cloud.

## 5. Numerical example

Now, let us demonstrate the usability of our MPM and DDMP implementations by means of a numerical example. Therefore, we simulate the penetration of a cone into soil. This is a common situation happening, for example, during the installation of a spudcan or a footing for a rig.

### *5.1. Model setup*

A numerical example of cone penetration into a cohesive soil similar to [18] is used. As shown in Fig. 1, a rigid cone with 60° angle is penetrated in a cohesive soil quasi-statically. A plane strain calculation is carried out for this model. The soil is undrained with a value of undrained shear strength $s_u$ of 3 kPa. The Young's modulus of the soil is set to $200s_u$. Tresca soil model is used. The dimension of the soil is 250 mm wide by 80 mm deep and the final penetration

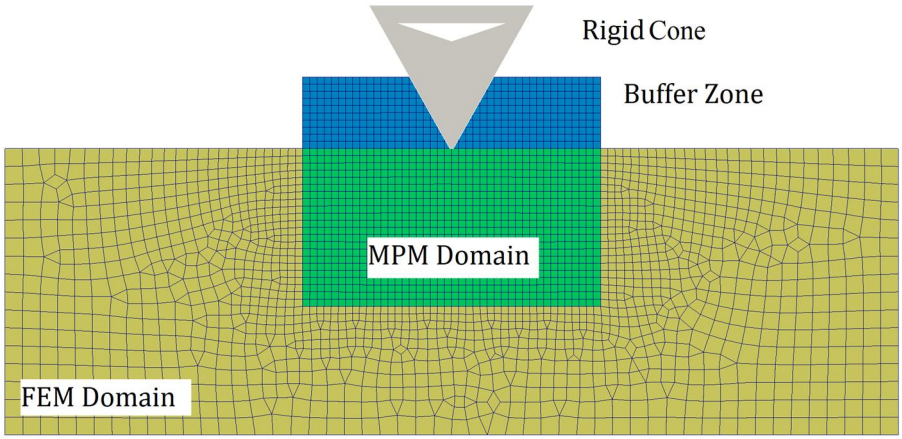


Fig. 1. Model setup.

depth of the cone is 30 mm. The penetration depth per step is set to 0.06 mm. The contact between the cone and the soil is set to smooth. To reduce the computation load, only one third of the middle strip with a depth of 45 mm is selected as the MPM domain. The remaining soil domain is analysed using FEM. A 20 mm thick buffer zone is created on top of the MPM domain to allow material point flow during the analysis. The mesh element size in the MPM domain is 2 mm, progressively coarsened to 5 mm at the boundaries in the FEM region. Initial material point density per element is 16.

The resistance force of the cone during penetration is observed. The force is normalised against the product of penetration width L of the cone and the undrained shear strength su, calculated by using the following equation:

$$N_c = \frac{F}{s_u L} \tag{19}$$

### *5.2. Improved accuracy of second-order MPM*

The normalised resistances of the cone in different penetration depths are shown in Fig. 2. The result from our second-order MPM with level-set contact formulation agrees very well with the LDFE result from [18].The accuracy of the result is also better than the MPM result from [18]. This improved accuracy is contributed from the use of second-order approximation in the computation domain as can be seen in Fig. 3, where we compare the normalised resistance at a penetration depth of 15 mm for several different meshes using first- and second-order MPM approximations.

Our results however, suffer from some numerical oscillation within the range of 2.5 mm to 8 mm penetration depths. This oscillation is partly caused by the inherent numerical noise from MPM analysis and the transition of MPM boundaries described by the level-set field. The magnitude of the oscillation is reduced in deeper penetrations because the contact surface area is increased, thus incorporating a more precise level-set boundary in the MPM domain. Further investigation is required to access the impact of the level-set field discretisation on the accuracy of the solution.

### *5.3. Second-order DDMP method*

Analysis using second-order DDMP yields smoother results in the range of 2.5 mm to 8 mm, as shown in Fig. 4. The oscillation, however, cannot be fully eliminated by the DDMP method because a part of the oscillation is contributed by the inaccurate level-set boundary approximation. This issue can be rectified by further mesh refinement or the use of a more accurate level-set definition. In the comparison between MPM and DDMP, it seems that DDMP is less accurate in the range of 3 mm to 6 mm. This might be caused by the stronger oscillation of MPM towards a local minima and is not a general characteristic of DDMP. Further study is needed to assess the effect of smoothing by DDMP on the accuracy of the solution.

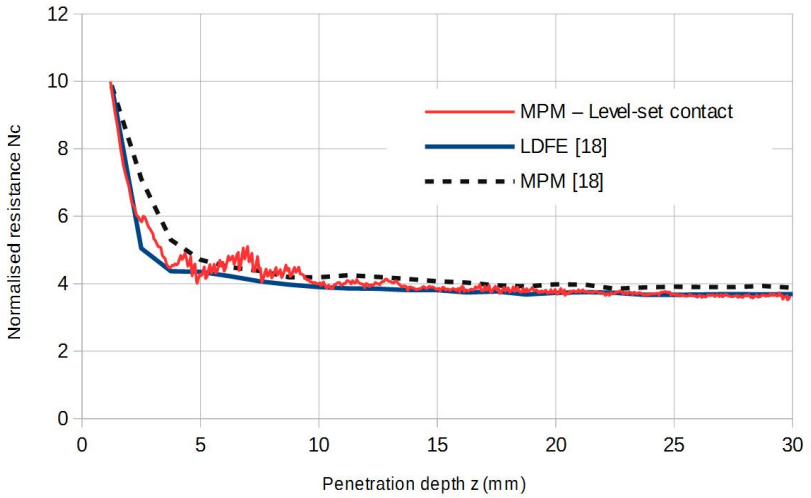


Fig. 2. Normalised resistances of the cone in different penetration depths.

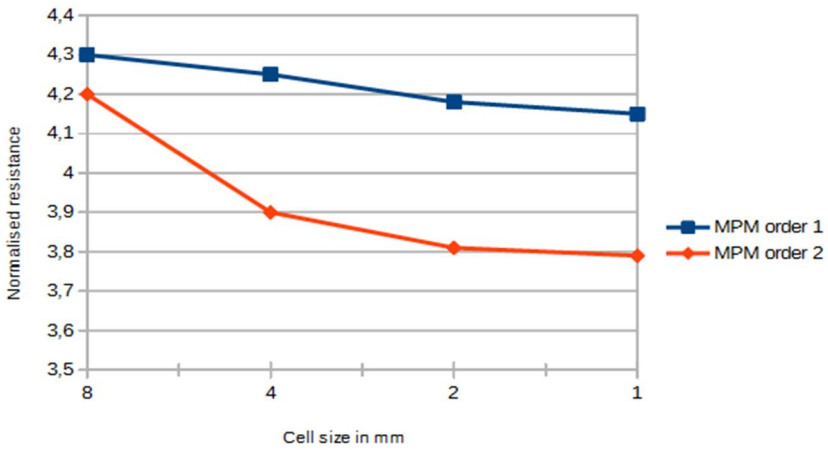


Fig. 3. Normalised resistance of cone at penetration depth 15 mm for different cell sizes.

## 6. Conclusion

We have presented new second-order MPM and DDMP Methods. In comparison to the conventional first-order MPM and DDMP method, they allow an easy employment of triangular and tetrahedral meshes without having to incorporate any additional measures to prevent locking. Further, they improve the accuracy of the numerical results.

At hand of some numerical examples, the successful application of the developed MPM and DDMP methods to a typical situation occurring in offshore geotechnical engineering was demonstrated.

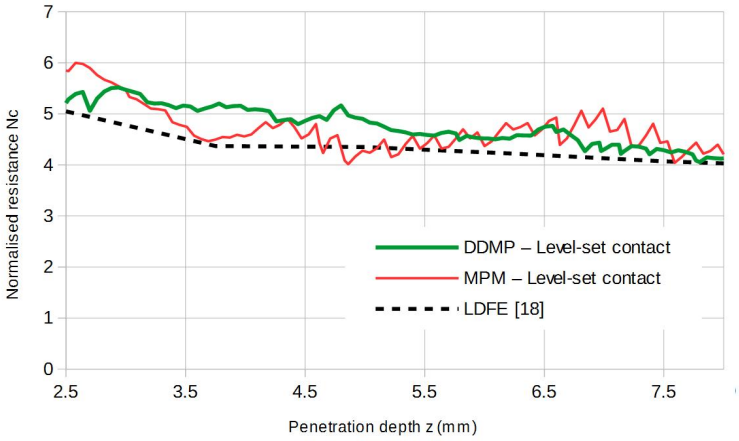


Fig. 4. Normalised resistances of the cone in different penetration depths for DDMP within the range of 2.5 mm to 8 mm.

## References

[1] Z. Więckowski, The material point method in large strain engineering problems, Comp. Meth. Appl. Engrg. 193 (2004), 4417–4438.
[2] L.J. Lim, A. Andreykiv, R.B.J. Brinkgreve, On the Application of the Material Point Method for Offshore Foundations, in: M.A. Hicks, R.B.J. Brinkgreve, A. Rohe (Eds.) Numerical Methods in Geotechnical Engineering (2014), Taylor & Francis, London, 253-258.
[3] W.T. Solowski, S.W. Sloan, Evaluation of material point method for use in geotechnics, Int. J. Numer. Anal. Meth. Geomech. 39 (2015), 685-701.
[4] M.A. Homel, R.M. Brannon, J.E. Guilkey, Simulation of shaped-charge jet penetration into drained and undrained sandstone using the Material Point Method with new approaches for constitutive modeling, In: E. Oñate, J. Oliver, A. Huerta (Eds.), CIMNE, Barcelona, 676-687
[5] H.H. Bui, R. Fukagawa, K. Sako, S. Ohno, Lagrangian meshfree particles method (SPH) for large deformation and failure flows of geomaterial using elastic-plastic soil constitutive model, Int. J. Numer. Anal. Meth. Geomech. 32 (2008), 1537-1570
[6] D. Sulsky, Z. Chen, H.L. Schreyer, A particle method for history-dependent materials, Comp. Meth. Appl. Mech. Eng. 118 (1994), 179-196
[7] L. Beuth, Formulation and application of a quasi-static material point method, PhD Thesis (2012), University of Stuttgart
[8] L.J. Lim, A. Andreykiv, R.B.J. Brinkgreve, Pile penetration simulation with material point method, In: M.A. Hicks, J. Dijkstra, M. Lloret-Cabot, M. Karstunen (Eds.) Installation effects in geotechnical engineering (2013), CRC Press, Boca Raton, FL, 24-30
[9] R.B.J. Brinkgreve, M. Bürg, A. Andreykiv, L.J. Lim, Beyond the Finite Element Method in Geotechnical Analysis, In: Numerische Methoden in der Geotechnik (2025), Bundesanstalt für Wasserbau, Karlsruhe
[10] T. Belytschko, W.K. Liu, B. Moran, Nonlinear Finite Elements for Continua and Structures (2000), Wiley, Chichester
[11] A. Ern, J.-L. Guermond, Theory and Practice of Finite Elements (2004), Springer, Heidelberg
[12] S.G. Brandenhagen, E.M. Kober, The generalized interpolation material point method, Comp. Model. Engrg. Sci. 5 (2004), 477-495
[13] D.Z. Zhang, X. Ma, P.T. Giguere, Material point method enhanced by modified gradient of shape function, J. Comp. Phys. 230 (2011), 6379-6398
[14] A. Sadeghirad, R.M. Brannon, J. Burghardt, A convected particle domain interpolation technique to extend applicability of the material point method for problems involving massive deformations, Int. J. Numer. Meth. Engrg. 86 (2011), 1435-1456
[15] A. Sadeghirad, R.M. Brannon, J.E. Guilkey, Second-order convected particle domain interpolation (CPDI2) with enrichment for weak discontinuities at material interfaces, Int. J. Numer. Meth. Engrg. 95 (2013), 928-952
[16] D. Sulsky, A. Kaul, Implicit dynamics in the material-point method, Comp. Meth. Appl. Mech. Engrg. 193 (2004), 1137-1170
[17] A. Andreykiv, F. van Keulen, D.J. Rixen, E. Valstar, A level-set-based large sliding contact algorithm for easy analysis of implant positioning, Int. J. Numer. Meth. Engrg. 89 (2011), 1317-1336
[18] J. Ma, D. Wang, M.F. Randolph, A new contact algorithm in the material point method for geotechnical simulations, Int. J. Numer. Anal. Meth. Geomech. 38(2014), pp. 1197-1210J. Van der Geer, J.A.J. Hanraads, R.A. Lupton, The art of writing a scientific article, J. Sci. Commun. 163 (2000), 51–59.